Medica-Plus: A Micromegas-based proof-of-concept detector for sub-becquerel tritium activity assessment at the service of oncological research

F. Jambon, S. Aune, P. Baron, T. Benoit, T. Bey, D. Desforge, E. Ferrer-Ribas, A. Grabas, M. Kebbiri, I. Mandjavidze, et al.

Medica-Plus: a Micromegas-based proof-of-concept detector for sub-becquerel tritium activity assessment at the service of oncological research

F. Jambon, S. Aune, P. Baron, T. Benoit, T. Bey, D. Desforge, E. Ferrer-Ribas, A. Grabas, M. Kebbiri, I. Mandjavidze, T. Papaevangelou, M. Riallot, M. Vandenbroucke

IRFU, CEA, Université Paris-Saclay, F-91191 Gif-sur-Yvette, France

F. Beau, V. Dive, C. Malgorn

JOLIOT, CEA, Université Paris-Saclay, F-91191 Gif-sur-Yvette, France

F. Malloggi, A. Rousselot

IRAMIS, CEA, Université Paris-Saclay, F-91191 Gif-sur-Yvette, France

F. Carrel, M. Trocmé

LIST, CEA, Université Paris-Saclay, F-91191 Gif-sur-Yvette, France

Abstract

To fulfill needs in oncological research a new Micromegas detector has been developed to follow radiolabelled drugs in living organisms at the single cell level. This article describes the proof-of-concept of such a detector and compares its ability to detect and assess sub-becquerel ^{3}H activities with a commercial β-imager.

Key words: MPGD, Micromegas, ^{3}H Radiolabelling

1. Introduction

Radio-labelling is one of the staple techniques to assess the behavior and biodistribution of drug candidates and their metabolites in pharmaceutical studies and development [1]. Tritium (^{3}H) and 14-Carbon (^{14}C) radio-labelling are still among first-choice technologies for labelling active compounds, especially when the precise quantification of drug targeting and excretion are required [2]. The field of oncology-related drug development is no exception to this rule, with maybe the additional constraint of tending towards lower doses due to the high toxicity of the drug itself [3]. Moreover, last decade discoveries in oncology highlighted the importance of cell heterogeneity on the drug affinity and metabolism [4], pushing further the need for precise quantification of drug, not only at the organ level, but also at the single-cell one.

In this context, the Medica-Plus project aims at developing a Micromegas-based [5] β-imager detector to assess sub-becquerel activities in single cells focussing on ^{3}H specifically. Biologists prefer ^{3}H for some applications as the chemistry and metabolism of the drug candidates is identical when substituting an atom like hydrogen by its radioactive counterpart as opposed to replacing it with fluorine. Radioactive labelling also conserves the drug molecule's conformation, also important for metabolism, which is not the case when attaching a fluorescent group for instance. Moreover the long half-life of ^{3}H (12 years) facilitates its use.

Standard techniques in β autoradiography are usually based on solid detectors like X-ray films or phosphors screens. These techniques need a two steps process: first exposure time and then off-line scanning. This two-steps process is time consuming and does not allow real-time acquisition. Gaseous detectors are particularly suited for β-imaging due to their low energy threshold, their good spatial resolution and their linearity. In addition they allow real-time

imaging. Instruments based on gaseous detectors exist. One example is the "Biospace Beta Imager 2000" [6] that will be used as our a reference detector. This imager implements a parallel plate proportional avalanche chamber with an optical readout [7]. Another example of gaseous detector using the charge readout mode is based on the Parallel Ionization Multiplier (PIM) [8, 9].

The Medica-Plus project involves a Micromegas-based detector. The advantages of the Micromegas detector with respect to the previously cited gaseous detectors are: the simplicity of the detector (and *in fine* the cost), the easiness of implementation and the gain in both sensitivity and in a fast response thanks to the auto-trigger electronics that optimises the signal-to-background ratio.

The overall project relies on a complex process of cell preparation in order to display unitary, well separated single-cells to be imaged in the detector that has been described elsewhere [10].

In the present article, we report improvements in the measurement of sub-becquerel activities with an optimized detector, coupled with strip-reading electronics, and its comparison with a commercial β-imager performances. Further optimisations of the detector design for the β-imaging of single cells will be presented in a later article.

2. Experimental set-up

In this section the Micromegas detection system, the sample choice and its manufacturing process and the activity assessment procedure are described in detail.

2.1. Detection setup

The detection system is based on the prototype detector that was described and characterized in detail here [10]. It consists of a Micromegas detector with an amplification gap of 128 µm, and a drift gap of 5 mm. The readout plane is

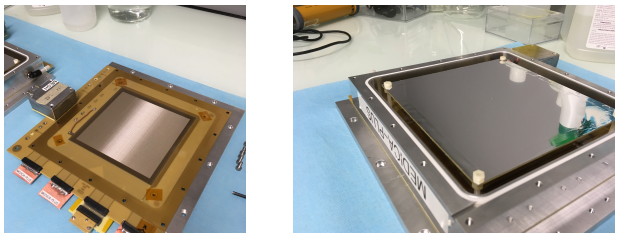

Figure 1: Photos of the detector. Left: The readout plane with the bulk mesh is visible. The active zone is $12.8 \times 12.8\,\mathrm{cm}^2$. Right: The mylar drift electrode mounted on the detector's chamber.

made of 256, 370 µm-large copper unidirectional strips with a 500 µm pitch. The detection gas mixture is 95% Argon - 5% Isobutane flown continuously. The drift cathode is a thin film of 50 nm-aluminized mylar from Goodfellow taut on a frame that adapts on drift supports allowing to maintain it in a given parallel position facing the reading plane. A picture of the the readout plane and the drift electrode is shown in Figure 1. The frame is maintained with a nuts and bolts system enabling for high voltage connection to the metallic face. This design was chosen so as to be able to minimize material waste when discarding the tritiated samples and the contaminated support to the appropriate waste management sector. In order to avoid readout plane contamination from samples that might drop on it, the detector is built so that the reading parts are always above the samples as can be seen in Figure 2.

The detector has been coupled with DREAM electronics [11], allowing for independent strip reading. The maximum gain measured with a ^{55}Fe source is ∼17000 [10]. The corresponding energy resolution (FWHM) is 29%.

The DREAM electronics is used in self-trigger mode, meaning that each of the 256 strips is able to generate a hit signal for data acquisition when the charge variation over a defined amount of time exceeds a defined threshold value. The results shown in this article were obtained with a threshold of 54 fC, to be compared to the dynamic range of 600 fC used during these tests.

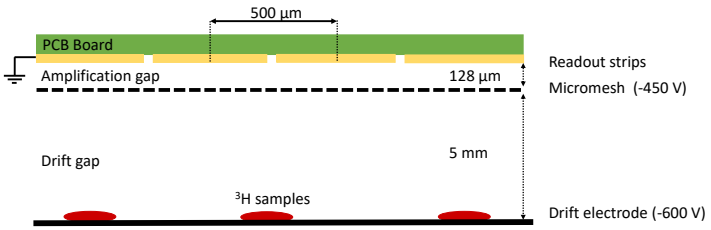

Figure 2: Sketch of the detector with its main characteristics. The Micromegas detector consists of an amplification gap of 128 µm and a drift gap of 5 mm. The readout plane is made of 256 strips with a pitch of 500 µm.

2.1.1. The reference detector: the commercial β-imager

A commercial Biospace Beta Imager 2000 (now renamed Biospace tRACER) has been used as a reference detector [6]. This imager is also a gaseous detector implementing a parallel plate proportional avalanche chamber with an optical readout [7] using a scintillating gas mixture (Argon-Triethylamine). The UV light emitted during the avalanche is recorded by a CCD camera. The β-imager adjusts its gain during the acquisition by modulating the high voltage applied internally depending on the activity present in the samples.

2.2. Tritium labelled samples

Instead of living tumor cells, tritiated glucose deposits with decreasing activities were used. Particular attention was given to the solution preparation. To avoid any change in the self-absorption, the total glucose concentration in each solution was kept constant and equal to the content of the most active solution, by adding non-radioactive glucose. Solutions of tritiated and classical labora-

tory D-glucose were prepared in a solvent made of 50% distilled water - 50% ethanol (98% purity, added for quicker drying time), with nominal activities of 0.185, 0.37, 1.85, 3.7, 18.5 and 37 Bq/μL.

The activity of the solutions was assessed by liquid scintillation counting using 100 μL samples to reduce the measurement uncertainty. Triplicate 5-minute counting using a commercial scintillation counter were made for each solution activity. The best standard deviation achieved was about 3%, which corresponds to the sum of systematic accuracy (one plastic tip is used per sample) and random error specification given by the pipette manufacturer. However the standard deviation could sometimes reach 15%. The corresponding measurements and its associated true standard deviation ("sigma") obtained for each batch are given in Table 2, in terms of activity per 1 μL droplet. The results will also be used as abscissa axis in the next section when comparing the measured activity with the deposited one. Also, in order to be consistent with the plots, the samples activities in the text will be expressed in terms of scintillation-counting assessed activity in the rest of the article.

The samples were deposited at the same time on the Micromegas drift cathode and on standard microscope glass slides. Samples were then left to dry before closing the detector or placing the slides in the β-imager cassette. To avoid any possible support material effect on the glucose cristallization process that might affect the beta-material interactions, the standard microscope glass slides were lined with the same aluminized mylar than the one used in the Micromegas detector. The support material effect has been assessed and is discussed briefly in Section 3.3, in which case the droplets were directly deposited on the glass slides.

For the Micromegas detector, two sets of μL droplets of solutions of each activity were deposited on the drift cathode. The total activity deposited is

thus 124.4 Bq. For reference, the lowest activity corresponds approximately to the expected cell ^{3}H activity for the cell-measurement campaign.

In order to assess the effect of the dynamic range on the beta-imager performance, two types of measurements were made. In the first measurement, samples with activities ranging from 36 Bq to 0.13 Bq per 1μL droplet were measured. This is referred as "Full Range" measurement in the text. In a second measurement, named "Reduced Range" measurement, a smaller dynamic range was tested : samples with activities ranging from 3.3 Bq to 0.13 Bq only were put in the detector. For each type of measurement, two droplets of each solution in the tested activity range were deposited on a glass support.

Three independent 30 min long measurements were performed with all six sample activities in the detectors in order to assess the accuracy, but also the standard deviation of the measurement for each detector. For the β-imager, another series of measurements was made only with the "lower activity range" samples inside (referred later as "Reduced" range, in opposition to "Full" range). The activity assessment methodology for each detector is described in the next section.

2.3. Activity analysis procedure

In this section, the activity assessment procedures for both detectors is detailed.

2.3.1. Micromegas data analysis

For the Micromegas measurement, all events triggering the DREAM electronics are recorded, and data is processed afterwards. First, pedestals are calculated and then subtracted for each individual strip. Common noise subtraction is performed by groups of 32 strips. Then, events of significant charge collected on neighbouring strips during a hit window are gathered together in

clusters. In this case, one cluster corresponds to one decay. A weighted arithmetic mean is computed on the distribution of charge amplitudes on each cluster strip, so that the cluster centre position could be assessed. Electronics noise is removed by a cut on low-amplitude clusters (Figure 3). This cut suppresses clusters with a maximum strip charge lower than twice the electronics threshold. Finally, a topological analysis is performed in order to keep only the clustered events compatible with ^{3}H -generated signal using two simple cuts. First, a minimum threshold is required on the energy of the larger contributing strip in a cluster; this discards large clusters with low energy, mainly coming from noisy background that would escape the common noise suppression. Second, only the signal collected in the DREAM electronics between 2 and 7 samples time stamps is kept (one sampling interval being approximately 48 ns long). Typical pulse shape of a tritium event is shown in Figure 4 left. The amplitude for the various strips of the cluster is shown as a function of time. Since the mean free path of the electron coming from the tritium decay is small (a few hundreds of microns), the events of interest will be narrow. The resulting clusters will be concentrated, they will not spread over more than 4 strips in space and more than 5×48 ns samples in time. Figure 4 right shows the distribution of time samples above threshold as a function of cluster centroid motivating the selection of sample time stamps described before. The overall effect of the data processing on the clusters charge distribution is shown in Figure 3 and 5, for a 30-minute long acquisition of ^{3}H -glucose samples in the Micromegas detector.

The activity of each ^{3}H -glucose sample is assessed by counting the number of clusters per peak, divided by the run length to obtain an activity in becquerel. A simple routine that fits a linear background over the whole distribution and detects the peaks from their local maximum has been developed. Each peak is fitted with a Gaussian function. The adjusted mean position and sigma are used

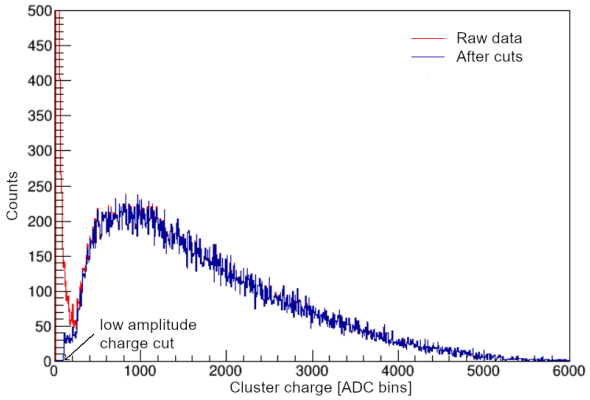

Figure 3: Effect of the data processing on the cluster charge distribution signal produced by a 30-minutes long measurement of ^{3}H -glucose samples; the β spectrum shape of the ^{3}H energy distribution is recognizable.

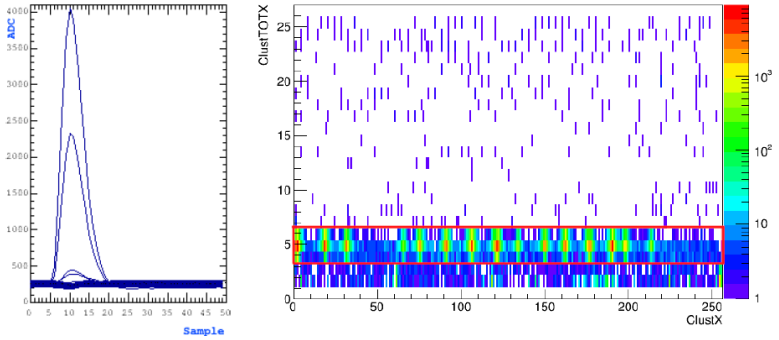

Figure 4: Left: Amplitude as a function of time sample for the strips of a cluster of a typical ^{3}H event. Right: Time samples above threshold as a function of cluster centroid. The cut on time samples between 2 and 7 is shown.

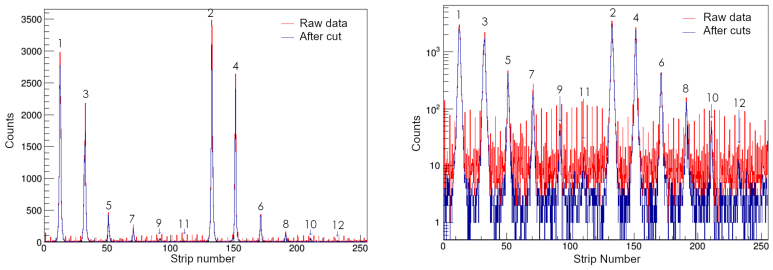

Figure 5: Reconstructed cluster position distribution produced by the ^{3}H -glucose samples during a 30-minute acquisition. Effect of the data processing on the result obtained. Left: linear count scale; Right: logarithmic count scale.

to calculate the number of clusters retained per peak. Cluster count per peak is the total bin content of the cluster centers distribution between the Gaussian fit mean parameter, plus or minus, five adjusted sigmas. A background subtraction is then performed using the calculated local background at mean peak position, considered constant along the peak width. The background before cuts is constant at 9 counts (5.0 mBq) per bin in raw data, and 5 counts (2.7 mBq) per bin after cuts.Therefore the value that has been subtracted for the estimation of the activity is 5 counts per bin over 6 bins.

The effect of this data treatment on the activity assessment is quantified on the right hand side of Table 1; the equivalent results obtained with the β-imager for both sample activity range conditions are displayed on Table 2 (associated data processing is detailed in Section 2.3.2). The activity determined without cuts or correction for each cluster peak is found in the "Raw" column; the "Cuts" column gives the activity after charge and topological cuts, while in the "Corrected" one, background subtraction is also applied. The peak numbers refer to those in Figure 5 for Micromegas (Figure 6 for the β-imager), while the "Scintillation counting" gives the expected activity of the 1 μL sample solution. Finally, "sigma" columns stand for the standard deviation obtained over the series of three measurements.

Peak	Scintillation		Micromegas			
Number	counting	sigma	Raw	Cuts	Corrected	sigma
1	36	6	11.75	11.55	11.53	0.20
2	36	6	11.57	11.30	11.28	0.17
3	21	4	7.20	6.96	6.95	0.09
4	21	4	7.57	7.30	7.28	0.03
5	3.3	0.4	1.49	1.28	1.26	0.04
5bis	3.3	0.4	-	-	-	-
6	3.3	0.4	1.58	1.36	1.34	0.02
6bis	3.3	0.4	-	-	-	-
7	1.48	0.08	0.97	0.71	0.70	0.03
7bis	1.48	0.08	-	-	-	-
8	1.48	0.08	0.70*	0.43*	0.41*	0.07
8bis	1.48	0.08	-	-	-	-
9	0.272	0.006	0.493	0.186	0.169	0.009
10	0.272	0.006	0.531	0.201	0.179	0.006
11	0.13	0.02	0.435	0.128	0.106	0.020
12	0.13	0.02	0.348	0.105	0.086	0.024

Table 1: Effect of data treatment and background subtraction on data for the Micromegas detector. Activities are in Bq. The significant digits are calculated over the series of three measurements of the same samples and correspond to the sigma column at the right of the activity for each measurement type, and to the error bars shown latter in plots.

*dead strip in the middle of the peak on the Micromegas detector. Not used for performance assessment

Peak	Scintillation		β-imager Corrected			
Number	counting	sigma	Full	sigma	Reduced	sigma
1	36	6	10	1	-	-
2	36	6	9	1	-	-
3	21	4	7	1	-	-
4	21	4	4	1	-	-
5	3.3	0.4	1.5	0.5	-	-
5bis	3.3	0.4	1.7	0.5	1.2	0.04
6	3.3	0.4	1.5	0.5	-	-
6bis	3.3	0.4	1.6	0.5	0.9	0.04
7	1.48	0.08	0.7	0.5	-	-
7bis	1.48	0.08	0.7	0.5	0.53	0.02
8	1.48	0.08	0.6	0.5	-	-
8bis	1.48	0.08	0.7	0.5	0.53	0.02
9	0.272	0.006	0.1	0.3	0.12	0.01
10	0.272	0.006	0.1	0.3	0.11	0.01
11	0.13	0.02	0.1	0.2	0.070	0.004
12	0.13	0.02	0.1	0.2	0.061	0.004

Table 2: Effect of data treatment and background subtraction on data for the β imager. Activities are in Bq. The significant digits are calculated over the series of three measurements of the same samples and correspond to the sigma column at the right of the activity for each measurement type, and to the error bars shown latter in plots. The background level for the chosen ROI is about 6 mBq.

2.3.2. β-imager activity analysis

For each measurement, the activity per sample is assessed as follows. First, the color scale is adjusted so that the sample contours are highly visible. An

illustration of the process is given on Figure 6; note that the apparent sample size look different due to the color scale. Then, samples are surrounded with a region of interest (ROI) where the total count of decay per mm^2 is calculated automatically by the β-imager software. Background noise is subtracted after choosing a similar ROI aside from the samples allowing the calculation of noise expressed in counts per mm^2. The corrected sample ROI value is then re-expressed in units of total counts, which are divided by the analysis time to obtain an activity in Bq. The results of activity assessment by the β-imager for both Full or Reduced (lower) activity range are given in Table 2. Since the background level for the chosen ROI is about 6 mBq, that is much smaller than the significant digits associated with the measurement, the detail of background subtraction effect is not given in Table 2.

3. Results and Discussion

In this section, a comparison of the overall activity assessment obtained with the Micromegas detector and with the commercial β-imager is presented. Then background correction and detection efficiency is discussed. Improvement perspectives are presented in the last subsection.

3.1. Comparison of ^3H activity assessment performance

In order to assess the measurement stability and reproducibility and separate it as much as possible from the sample-to-sample variation for a same tritiated solution batch, a two-step process has been applied. First, for each sample/deposit, the mean activity and the associated standard deviation over three independent 30 min measurements are calculated. This exposure time was chosen carefully so that the detectors would be able to separate clearly the signal from the background for the lowest activity tested in the study, but not more. As a beneficial side effect, short exposure-time is also a way to assess

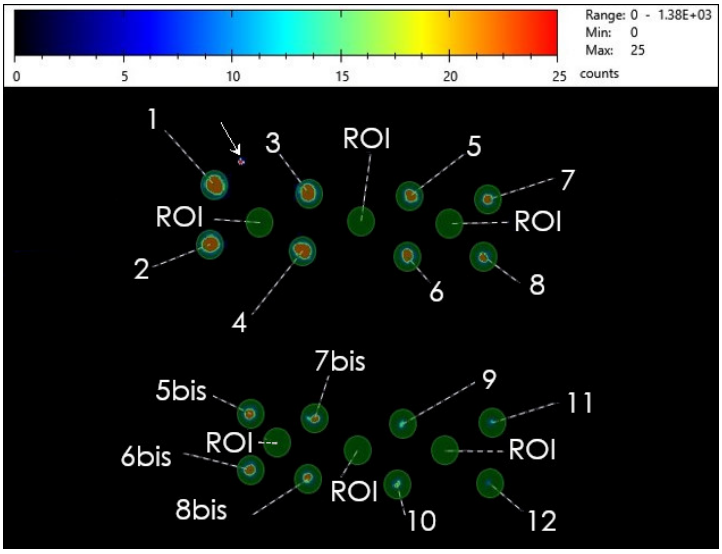

Figure 6: Illustration of the β-imager activity assessment analysis for a "Full Range" measurement. Spots are numbered according to the activities of peaks in Figure 5 for consistency. ROI stands for Region Of Interest chosen for background estimation. The arrow (close to spots 1 and 3) points a hotspot, that might be a contamination on the support of the grid. For the Reduced Range measurement, only the bottom spots were counted.

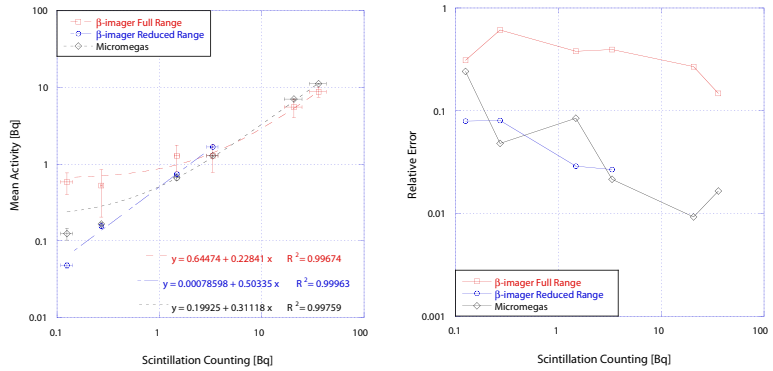

Figure 7: Right: Comparison of mean activity assessment (symbols) by a commercial β-imager for two measurements with different ranges of activities and by the Micromegas detector, linear regressions associated (lines and equations). Left: Relative error made by the detectors in different conditions versus sample activity.

short exposure time stability. Then a mean of the means, representing the activity accuracy and its combined error are calculated. The error represents a measurement-to-measurement deviation and thus an indicator of reproducibility quality.

The activities thus obtained are plotted versus the sample activity derived from the scintillation counting of the ^{3}H -glucose solution batch, and displayed in Figure 7. A comparison of the results obtained with the full dynamic range of samples with the Micromegas (black lozenges) and the commercial β-imager (red squares) as well as the recounting of the Reduced (bottom half) range of activities with the β-imager (blue circles) is displayed. The vertical error bars (see "sigma"s in Table 2) are the two-step standard deviation calculated as described above, while the horizontal ones correspond to the scintillation counting standard deviation. A linear regression is also plotted and the fitted parameters and associated R^2 are displayed in the figure. The slope is a measurement of the apparent detection efficiency while the constant parameter is an evaluative of the theoretical detection limit. In order to help evaluate the differences between

each detector and conditions, a graph of the relative error, that is the ratio of the standard deviation over the mean value, is plotted Figure 7 left.

First, comparing the activity assessment through in broad outline, and from the linear regression from Figure 7, it is clear that, overall, for the full range of sample activity, the Micromegas-based detector (black curve, lozenges) does better than its commercial counterpart (red curve, squares) when used in the Full range measurement. Indeed, the Micromegas detector data is associated with a better detection yield, linearity and projected detection limit. Also, the relative error associated with the activity assessment is better with the Micromegas detector: one to two orders of magnitude compared to one of the commercial β-imager with the Full range measurement (Figure 7 left). When looking at the "reduced range measurement" of the beta-imager, the detection yield and the error on the activity are comparable to the ones obtained with the Micromegas.

3.2. Background noise and optimal detection strategies

In the case of the Micromegas detector, since each cluster is treated as a decay, the detector is used in counting mode. The gain setup chosen for optimal performance remains fixed so that the detection of a given event does only depend on its energy.

This is different from how the commercial β-imager works as explained in Section 2.1.1. As the gain is adjusted depending on the activities present in the samples, for low activities, this results in an oscillation of its background level during the acquisition time, specially for the "reduced range measurements", and eventually in sparks on the sample that can induce errors or in the worst case detrimental effects on the detector itself including contamination. An illustration of this oscillation process is given in Figure 8 where the relative count rate around average for a one-hour acquisition has been plotted for both detec-

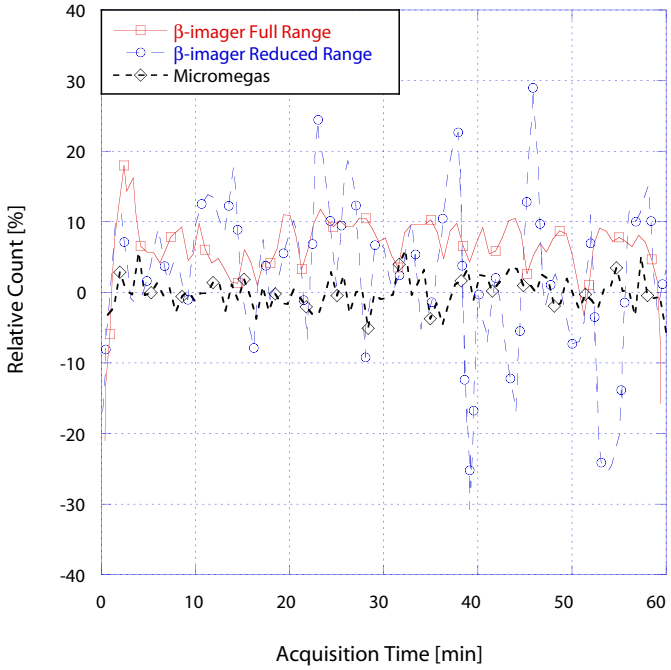

Figure 8: Relative detector count rates for a 1-hour acquisition : comparison between β-imager Full (red squares) and Reduced (blue circles) dynamic ranges and Micromegas (black lozenges).

tors.

For this reason there is a strong effect of the dynamic range on the activity assessment, especially at low activity. As a result, the situation where spot-like samples have a broad range of activities in unfavourable for the commercial β-imager, while the Micromegas detector offers a more reproducible and stable measurement even for short acquisitions times.

Considering the background rate roughly constant and resulting essentially from the interaction of cosmic particles with the detector, it is a good strategy to correct the measurement with an average of the background. However, this

induces a disadvantage in situations where the signal-to-background ratio is low (in the present case, this means at low samples activity). As a result, the commercial β-imager is disadvantaged when measuring the Full range of samples activities: as explained, its gain is set "low" and the signal-to-background ratio is lower than the best achievable one, because low energy clusters associated with ^{3}H decay are not detected, whereas the cosmic particles-related tracks are. As a consequence, the error, especially on small activity samples, is high. On the other hand, for the Reduced (and lower) range of activities, the commercial imager sets a high gain and gets a better signal-to-background ratio, and does better than the Micromegas.

3.3. Apparent efficiency of the detectors

In the series of tests presented in the previous section, the apparent efficiency is 31% on mylar (Micromegas) or 23% on mylar-on-glass (β-imager). The efficiency on mylar on glass is only higher (50%) in the case of reduced dynamic range, for which the β-imager actually sets up a higher high voltage between sample and grids.

This added to a likely combination of good background estimation and subtraction may explain this difference.

Figure 9(a) also demonstrates graphically a strong sample-to-sample variation in the local distribution of the activity. This dependence for the crystallization pattern is one of the motives for way the two-step mean and standard deviations described in the previous section.

To summarize, working with ^{3}H -glucose is a handy, quick and easy way to develop the Micromegas-based detector proof-of-concept and show its ability to detect and assess low ^{3}H activities. But the crystallization process sets up limitations that cannot be fully overcome nor compensated by a simulation work for instance.

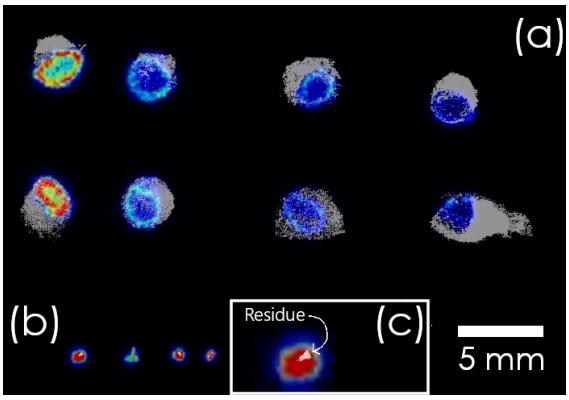

Figure 9: Distribution on glass only (a) versus aluminized mylar on glass (b) support of crystallized matter (grey) versus radioactivity (color) seen in the commercial β-imager. Insert (c) : a zoom of the most active sample on mylar. Four sample activities are tested, one per column; the activity ratio from right to left is 1:5

3.4. Perspectives for improvement

For the Micromegas-based detector, several domains of improvement exist, that can be attained by successive steps of background treatment, detector optimization, cosmics rejection. They are represented in Figure 10, where the "Assessed Activity" curve is plotted according to the Micromegas linear regression fit from the previous section. Considering that the Micromegas detection efficiency is constant, improvement consists in getting closer to the straight "Efficient, noise-less" line that has the same slope, but no constant parameter. The "Current Background" level was calculated from the data of the previous section, considering a 7-bin large cluster.

The most potent improvement is probably the post-process rejection of the background and the treatment of noise. At the moment it is very simplistic and is based on a simple linear background fitting that is not optimal for short acquisition times like in the present test, because the actual number of counts due to cosmic contribution is low and does not average well across the detector strips. One also expects an improvement on the background rejection by op-

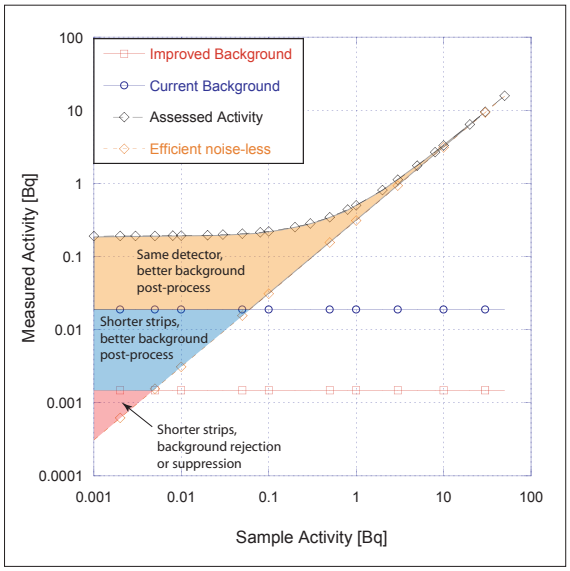

Figure 10: Domains of improvement considering the current activity assessment function of the Micromegas versus a potential perfectly noise-less detector with the same efficiency.

timising the topological selection of tritium-related events. Coincidence muon rejection could also bring the background even closer to zero, strip-wise. An extended area of possible better results exists, on the orange and blue areas of Figure 10.

A further step consists in optimizing the detector geometry. At the moment, due to the long unidirectional strips of the reading plane, the background due to noise and cosmic contributions is very high compared to the signal coming from the samples, because the former is integrated over the whole strip length ($\sim 12\,\mathrm{cm}$). As a result, the use of shorter strips or of pads would drastically decrease the background level. This hypothesis is represented by the "Improved Background" line that was obtained by applying a ratio of 1/12 to the Current Background one. Furthermore, using single pads dedicated to each single cell activity measurement could be beneficial, in the sense that all the events clusters

would face a metallic detection area to collect them on the readout plane.

Finally, to improve further the detection sensitivity of the Micromegas-based detector, background could be rejected by classical anti-coincidence techniques (red area in Figure 10).

To summarize, several improvement strategies are foreseen to improve the detector. In the case where the tumoral cells activity would be lower than the lowest sample activity considered in this paper (0.3 Bq), the Micromegas-based detector still has some practical moves to make to perform the task.

4. Conclusion

The performance of a new Micromegas-based detector aiming at fulfilling new needs in oncological research has been tested. Its ability to assess sub-becquerel ^{3}H activities has been investigated and compared with a commercial β-imager. For this, ^{3}H -glucose was used as a convenient, scalable dummy sample. Activity assessment, linearity and stability from sub-becquerel (0.1 Bq) to a few tens of becquerels (36 Bq) per spot have been estimated in a comparative measurement of samples originating from the same ^{3}H -glucose solutions.

Overall and in the presence of a broad dynamic range of activities, the Micromegas-based detector proved to do better than its commercial counterpart. The observed detection efficiency is constant at 31% for the Micromegas detector and 23% (with "Full Range" measurements) and 50% (with "Reduced Range" measurements) respectively for the β-imager. Finally, for the present sample size of several hundreds of microns, background treatment (in conjunction with the unfavourable readout plane geometry) sets the difference between the detectors. Next steps will concern the measurement of biological tumor samples with an upgraded detector allowing for single cell array deposition with an optimised readout plane. Those smaller samples might separate more thoroughly both

detector performances, since the image treatment by the commercial β-imager might hinder its acquisition process.

Acknowledgments

The authors acknowledge the financial support of the Cross-Disciplinary Program on Instrumentation and Detection of CEA, the French Alternative Energies and Atomic Energy Commission and the support of the P2I Department of Paris-Saclay University.

References

[1] N. Penner, L. Xu, C. Prakash, Radiolabeled absorption, distribution, metabolism, and excretion studies in drug development: Why, when, and how?, Chemical Research in Toxicology 25 (3) (2012) 513–531, pMID: 22309195. arXiv:https://doi.org/10.1021/tx300050f, doi:10.1021/tx300050f.
URL https://doi.org/10.1021/tx300050f

[2] E. M. Isin, C. S. Elmore, G. N. Nilsson, R. A. Thompson, L. Weidolf, Use of radiolabeled compounds in drug metabolism and pharmacokinetic studies, Chemical Research in Toxicology 25 (3) (2012) 532–542, pMID: 22372867. arXiv:https://doi.org/10.1021/tx2005212, doi:10.1021/tx2005212.
URL https://doi.org/10.1021/tx2005212

[3] R. Lowenthal, K. Eaton, Toxicity of chemotherapy, Hematology/Oncolog Clinics of North America 10 (4) (1996) 967. doi:https://doi.org/10.1007/s11307-017-1144-0.

[4] A. Marusyk, V. Almendro, K. Polyak, ntra-tumour heterogeneity: a looking

glass for cancer?, Nat. Rev. Cancer 12 (2012) 323–334. doi:https://doi.org/10.1038/nrc3261.

[5] Y. Giomataris, P. Rebourgeard, J. P. Robert, G. Charpak, MICROMEGAS: A High granularity position sensitive gaseous detector for high particle flux environments, Nucl. Instrum. Meth. A376 (1996) 29–35. doi:10.1016/0168-9002(96)00175-1.

[6] Biospacelab, https://biospacelab.com/products/#autoradiography.

[7] N. Barthe, K. Chatti, P. Coulon, S. Maîtrejean, B. Basse-Cathalinat, Recent technologic developments on high-resolution beta imaging systems for quantitative autoradiography and double labeling applications, Nuclear Instruments and Methods in Physics Research Section A: Accelerators, Spectrometers, Detectors and Associated Equipment 527 (1) (2004) 41–45, proceedings of the 2nd International Conference on Imaging Technologies in Biomedical Sciences. doi:https://doi.org/10.1016/j.nima.2004.03.014.
URL https://www.sciencedirect.com/science/article/pii/S0168900204003614

[8] L. Luquin, et al., Parallel Ionization Multiplier (PIM): Application of a new concept of gaseous structure to tracking detectors, Nucl. Instrum. Meth. A 518 (2004) 135–138. doi:10.1016/j.nima.2003.10.042.

[9] J. Donnard, D. Thers, N. Servagent, L. Luquin, High spatial resolution in β-imaging with a PIM device, in: 2007 IEEE Nuclear Science Symposium and Medical Imaging Conference, IEEE Nucl.Sci.Symp.Conf.Rec., 2007, pp. 4658–4661. doi:10.1109/NSSMIC.2007.4437146.

[10] F. Jambon, E. Ferrer-Ribas, F. J. I. Gutierrez, F. Beau, V. Dive, F. Malloggi, A. Rousselot, F. Carrel, M. Trocmé, Medica-plus: a novel micromegas

detector for high-resolution *beta* imaging for improved pharmacological applications, Journal of Physics: Conference Series 1498 (2020) 012046. doi:10.1088/1742-6596/1498/1/012046.
URL https://doi.org/10.1088%2F1742-6596%2F1498%2F1%2F012046

[11] A. Acker, D. Attié, S. Aune, J. Ball, P. Baron, Q. Bertrand, D. Besin, T. Bey, F. Bossù, R. Boudouin, M. Boyer, G. Christiaens, P. Contrepois, M. Defurne, E. Delagnes, M. Garçon, F. Georges, J. Giraud, R. Granelli, N. Grouas, C. Lahonde-Hamdoun, T. Lerch, I. Mandjavidze, O. Meunier, Y. Moudden, S. Procureur, M. Riallot, F. Sabatié, M. Vandenbroucke, E. Virique, The CLAS12 Micromegas Vertex Tracker, Nucl.Instrum.Meth.A 957 (2020) 163423. doi:10.1016/j.nima.2020.163423.
URL https://hal.archives-ouvertes.fr/hal-02483901

Credit Author Statement

Medica-Plus: a Micromegas-based proof-of-concept detector for sub-becquerel tritium activity assessment at the service of oncological research

F. Jambon, conceptualization, methodology, software, resources, formal analysis, investigation, software, data curation,visualization, Writing - Original Draft

S. Aune, resources

P. Baron, investigation, resources, formal analysis

T. Benoit, resources

T. Bey, resources

D. Desforge, resources

E. Ferrer-Ribas, conceptualization, methodology, formal analysis, writing - Original Draft, supervision, funding acquisition

A. Grabas, resources,software

M. Kebbiri,, resources

I. Mandjavidze, investigation, resources, formal analysis**,** Writing - Review & Editing,

T. Papaevangelou, visualisation, resources, formal analysis Writing - Review & Editing,

M. Riallot, resources

M. Vandenbroucke, investigation, resources**,** software, formal analysis, Writing - Review & Editing

F. Beau, investigation, resources, formal analysis

V. Dive, conceptualisation, Project administration, Funding acquisition

C. Malgorn, investigation, resources

F. Malloggi, methodology, conceptualisation, Funding acquisition

A. Rousselot, methodology, investigation, resources

F. Carrel, conceptualisation, funding acquisition

M. Trocmé methodology, resources, Writing - Review & Editing